

Transient-grating single-shot supercontinuum spectral interferometry (TG-SSSI)

S. W. Hancock, S. Zahedpour, H. M. Milchberg

Institute for Research in Electronics and Applied Physics, University of Maryland, College Park, Maryland, 20742, USA

Abstract: We present a technique for the single-shot measurement of the space- and time-resolved spatiotemporal amplitude and phase of an ultrashort laser pulse. The method, transient-grating single-shot supercontinuum spectral interferometry (TG-SSSI), is demonstrated by the space-time imaging of short pulses carrying spatiotemporal optical vortices (STOVs). TG-SSSI is well-suited for characterizing ultrashort laser pulses that contain singularities associated with spin/orbital angular momentum or polarization.

I. Introduction

The need to characterize ultrashort laser pulses has spawned a large and increasing number of single-shot techniques including autocorrelation [1], multiple versions of frequency resolved optical gating (FROG) [2-6], spectral phase interferometry for direct electric-field reconstruction (SPIDER) and related methods [7-12], STRIPED FISH [13], d-scan [14], plus single-shot supercontinuum spectral interferometry (SSSI) [15-17] and other spectral interferometry methods [18,19]. While the basic FROG and SPIDER techniques extract only the space-independent temporal amplitude and phase, more complicated techniques [12-14] have recovered the *spatiotemporal* phase and amplitude of a laser pulse in a single-shot, albeit only with simple features such as pulsefront tilt. STRIPED-FISH [13] and d-scan [14] methods use iterative algorithms which, to our knowledge, have not been shown to converge for complicated structured light containing singularities, and SEA-SPIDER requires ancillary assumptions in determining the timing of spatial slices [12]. While SSSI does not recover the spatiotemporal phase of a pulse, it does recover the spatiotemporal pulse envelope, which has enabled measurement of ionization rates and ultrafast plasma evolution [20], electronic, vibrational and rotational nonlinearities [21,22], as well as nonlinear refractive indices and pulse front tilt [23].

In this paper, we present a new method that can measure, in a single-shot, the spatiotemporal phase and amplitude of an ultrafast laser pulse. It was developed for recent measurements [24] of pulses embedded with spatiotemporal optical vortices (STOVs) [25] and is well-suited for characterizing ultrashort laser pulses that contain singularities associated with spin/orbital angular momentum (SAM/OAM) [26-28] or polarization [29].

II. Experimental Setup

We first briefly review SSSI by examining three of the beams in Fig. 1: the “structured pulse” E_S which we want to measure, the reference pulse E_{ref} , and the probe pulse E_{pr} . Here, the structured pulse has spatiotemporal phase and amplitude imposed by the zero dispersion $4f$ pulse shaper [30-32] in the lower left of the figure. The reference and probe supercontinuum (SC) pulses are generated upstream of Fig. 1 by filamentation in a 2 atm SF₆ cell followed by a Michelson interferometer (not shown), with E_{ref} leading

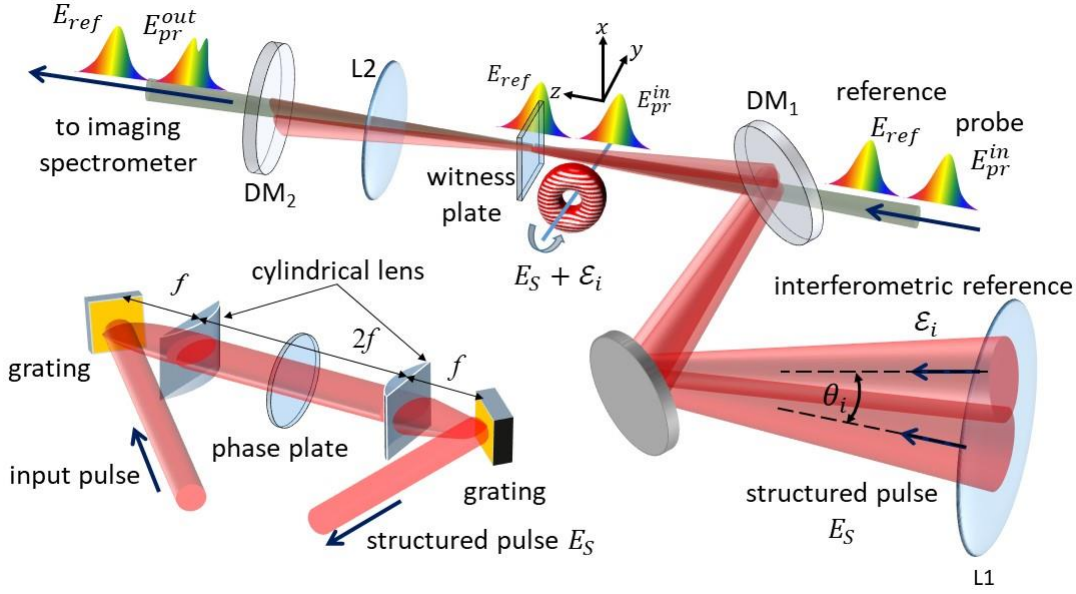


Fig. 1. Setup for transient grating single-shot spectral interferometry (TG-SSSI). The structured pulse E_S and the interferometric reference pulse E_i cross at angle θ_w at the focus of lens L1 in a fused silica witness plate (θ_i in air), where a transient grating is formed. The grating is probed by a supercontinuum (SC) probe E_{pr}^{in} , preceded ~ 2 ps earlier by a reference SC pulse E_{ref} . Imaged by L2, E_{ref} and E_{pr}^{out} interfere at an imaging spectrometer and the interferogram is analyzed in the Fourier domain, yielding a single-shot time and space resolved image of amplitude and phase of E_S . *Bottom left:* $4f$ pulse shaper [30–32] for generating spatiotemporally structured pulses E_S , here STOVs [24,33,34] imposed on a 50 fs, $\lambda=800$ nm input pulse. The STOV phase windings are imposed by $l = \pm 1$, and $l = -2$ spiral phase plates in the Fourier plane of the pulse shaper. The phase plates are etched on fused silica and have 16 levels (steps) every 2π .

E_{pr} by ~ 2 ps. The transient amplitude of E_S is measured via the phase modulation it induces in a spatially and temporally overlapped SC probe pulse E_{pr} in an instantaneous Kerr “witness plate”, here a thin (100–500 μm) fused silica window. The resulting spatio-spectral phase shift $\Delta\phi(x, \omega)$ imposed on the probe is extracted from interfering $E_{pr}^{out} \sim \chi^{(3)} E_S E_S^* E_{pr}^{in}$ with E_{ref} in an imaging spectrometer. Here, E_{pr}^{in} and E_{pr}^{out} are the probe fields entering and exiting the witness plate, $\chi^{(3)}$ is the fused silica nonlinear susceptibility, and x is position within a 1D transverse spatial slice through the pump pulse at the witness plate (axes shown in Fig. 1). Fourier analysis of the extracted $\Delta\phi(x, \omega)$ [20] then determines the spatio-temporal phase shift $\Delta\phi(x, \tau) \propto |E_S(x, \tau)|^2 \propto I_S(x, \tau)$, yielding the 1D space + time spatio-temporal intensity envelope I_S .

Measurement of the spatiotemporal phase of E_S is enabled by the addition of an interferometric reference pulse E_i , which is crossed with E_S at a small angle θ_i ($\theta_w = 3.15^\circ$ in the witness plate). This forms a nonlinear transient refractive index grating, where E_i has the same center wavelength as E_S but is bandpassed to be temporally longer. The transient grating (TG) is now the signal probed by SSSI (yielding the new method we call TG-SSSI), where the output probe pulse from the witness plate becomes $E_{pr}^{out} \propto \chi^{(3)} E_S E_i^* E_{pr}^{in}$. The interference of E_{pr}^{out} and E_{ref} in the imaging spectrometer then enables extraction of $\Delta\phi(x, \omega)$, yielding $\Delta\phi(x, \tau)$ as before. We note that $\Delta\phi(x, \tau)$ is the envelope of E_S modulated by the transient grating: $\Delta\phi(x, \tau) \propto I_S(x, \tau) f(x, \tau)$, where $f(x, \tau) = \cos(2k_w x \sin(\theta_w/2) + \Delta\Phi(x, \tau))$ is the transient grating, $k_w = n_0 k$ is the pump central wavenumber in the witness plate, $n_0 = 1.45$, and $\Delta\Phi(x, \tau)$ is the spatiotemporal phase of E_S .

In the analysis of the 2D $\Delta\phi(x, \tau)$ images, $\Delta\Phi(x, \tau)$ is extracted using standard interferogram analysis techniques [13,14], and $I_S(x, \tau)$ is extracted using a low pass image filter (suppressing the sidebands imposed by the transient grating). Due to group velocity mismatch in the witness plate between E_S (centre wavelength $\lambda_0 = 800$ nm) and the SC probe ($\lambda_{pr} = 600$ nm), the extracted phase shift is smeared slightly in time by ~ 4 fs per $100\mu\text{m}$ of fused silica.

The laser used in the experiments is a 4 mJ/pulse, 50 fs FWHM, $\lambda_0 = 800$ nm, 1 kHz Ti:Sapphire system. The beam is split 3 ways, with ~ 100 μJ directed to SC generation (400-700nm) for E_{pr} and E_{ref} , and a portion of the rest for E_S and E_i , whose energies were controlled using $\lambda/2$ plates and thin-film polarizers. The structured pulse E_S was embedded with spatiotemporal phase windings by placing $l = \pm 1$ or $l = -2$ spiral phase plates at the Fourier plan of the $4f$ pulse shaper [24].

As depicted in Fig. 1, the SC reference and probe pulses, E_{ref} and E_{pr}^{in} , are combined collinearly with the pulse E_S using dichroic mirror DM_1 , with E_S , E_i , and E_{pr}^{in} overlapping temporally in the witness plate, while E_{ref} precedes them (by 2 ps). From the output face of the witness plate, E_{ref} and E_{pr}^{out} were magnified and relay imaged onto the spectrometer slit using high numerical aperture (NA) telescope with achromatic lenses. The large NA is necessary to collect the first order diffraction ($m = \pm 1$) of E_{pr}^{out} from the transient grating. It is important for the imaging lenses to be achromatic for the image at the spectrometer slit to be in focus for all SC wavelengths and to minimize spherical aberration, which could spatially offset the diffracted orders of E_{pr}^{out} from the zero order. Background and signal data were collected at 40 Hz by placing

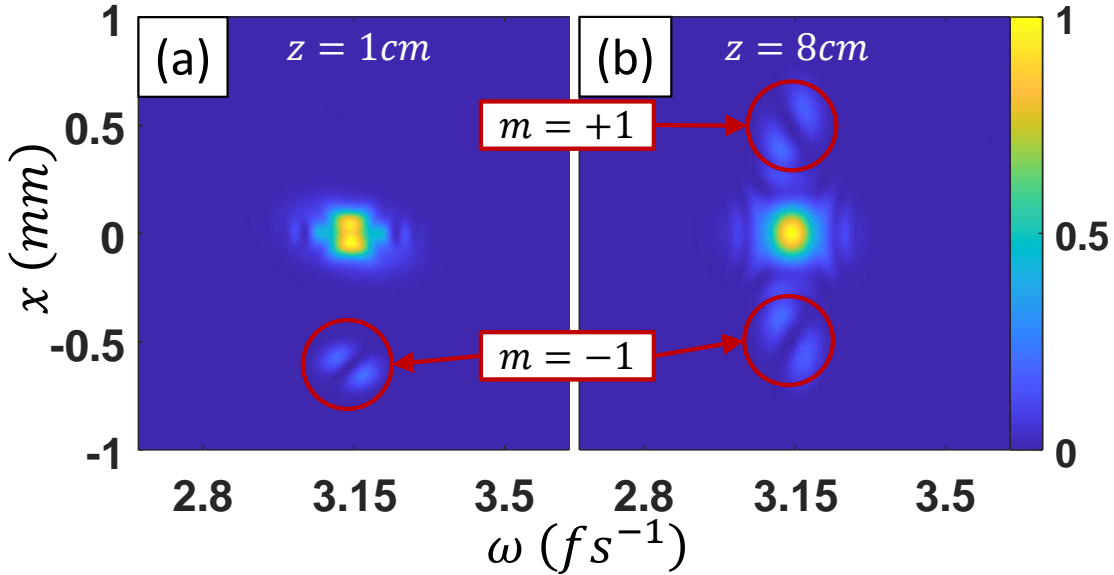


Fig. 2. Simulated spectrally-resolved scattering of supercontinuum probe pulse E_{pr} from a transient nonlinear grating in a $500 \mu\text{m}$ thick fused silica plate, generated by the interference of pulses E_S and E_i , where z is distance from the output face of the plate. Plotted as $|\Delta E_{pr}|^2 = |E_{pr}^{out} - E_{pr}^{in}|^2$. (a) Bragg regime transient grating: $\theta_w = 3.15^\circ$, grating period $\Lambda = 10\mu\text{m}$, and $Q = 13.0$. Here, the scattering is captured at $z = 1$ cm owing to the rapid escape of the single diffracted order ($m = -1$) from the simulation window. (b) Raman-Nath regime transient grating: $\theta_w = 0.31^\circ$, $\Lambda = 100\mu\text{m}$, and $Q = 0.13$, showing $m = \pm 1$ diffraction orders.

a chopper in the path of E_S , which allowed for the subtraction of the phase shift induced by \mathcal{E}_i in the witness plate.

In principle, achromatic imaging of all diffracted orders precludes the need for detailed analysis of the diffraction. However, it is interesting to note that in our experiment, we observe only the zero order ($m = 0$) and the $m = -1$ order diffraction of the probe. To understand this, we assess whether probe diffraction is in the Bragg regime (one dominant diffraction peak) or in the Raman-Nath regime (multiple positive and negative diffraction orders) [35] by considering the dimensionless parameter $Q = 2\pi\lambda_i L / \Lambda^2 \bar{n}$, where λ_i is the vacuum wavelength of incident light, Λ is the interference grating period, \bar{n} is the mean refractive index, and L is the grating thickness. From ref. [35], diffraction is in the Raman-Nath regime for $Q \leq 1$ and in the Bragg regime for $Q \gg 1$. Our TG-SSSI configuration (with a $l = 500 \mu\text{m}$ fused silica witness plate, $\Lambda(\theta_w = 3.15^\circ) = 10 \mu\text{m}$, $n_2 = 2.5 \times 10^{-16} \text{ cm}^2/\text{W}$, and $\bar{n} = n_0 + n_0 n_2 l = n_0 + \Delta\phi_{TG}/kL$, where $\Delta\phi_{TG}$ is the modulated phase shift amplitude of the transient grating) gives $Q \cong 13.0$, which is in the Bragg regime. (Both $\Delta\phi_{TG}$ and Λ are from our measurements.) This explains the observation of only one diffracted order.

This result is confirmed by simulations of scattering of E_{pr} from the nonlinear grating formed by the interference of E_S and \mathcal{E}_i . The simulation uses our implementation [36] of the unidirectional pulse propagation equation (UPPE) method [37], where all 3 beams intersect in the $500\mu\text{m}$ thick fused silica plate (with E_S and \mathcal{E}_i crossing at angle θ_w and E_{pr}^{in} normal to the surface). The beam parameters are E_S ($\lambda=800\text{nm}$, 50 fs FWHM, $w_0 = 100\mu\text{m}$, $I_{s,peak} = 28 \text{ GW}/\text{cm}^2$, $l = +1$ STOV), \mathcal{E}_i ($\lambda=800\text{nm}$, 300 fs FWHM, $w_0 = 300\mu\text{m}$, $I_{i,peak} = 28 \text{ GW}/\text{cm}^2$, GDD = 0 fs²), and E_{pr}^{in} ($\lambda = 600\text{nm}$, $\Delta\lambda = 350\text{nm}$, 2.4 ps FWHM, $w_0 = 500\mu\text{m}$, GDD = 1200 fs², TOD = 200 fs³). The output electric field is numerically propagated 4 cm beyond the witness plate in air and then E_S and \mathcal{E}_i are spectrally filtered out, leaving the field E_{pr}^{out} . Figure 2(a) shows simulation results of probe diffraction for conditions similar to our experimental parameters ($\theta_w = 3.15^\circ$ and $Q = 13.0$), where only the $m = -1$ diffraction order is present (Bragg regime), agreeing with our experiments. The crossing angle for Fig. 2(b) was chosen to be $\theta_w = 0.31^\circ$, giving $Q = 0.13$, in the Raman-Nath regime, and the $m = \pm 1$ orders are present. We note that our current TG-SSSI setup could be adjusted to operate in the Raman-Nath regime by increasing the grating period Λ (to $\Lambda \geq \sqrt{2\pi\lambda_i L / \bar{n}}$), but increasing the intensity of E_S or \mathcal{E}_i to increase n_1 could result in non-negligible plasma formation in the witness plate and refractive distortion of E_{pr} .

Figure 3(a) shows an example of a raw TG-SSSI interferogram frame recorded on the imaging spectrometer camera. Here, the pulse shaper generates E_S as a $l = -2$ spatiotemporal optical vortex (STOV) pulse [24,25]. The vertical spectral fringe spacing is set by the Michelson-imposed time delay between the E_{ref} and E_{pr}^{out} pulses. The 2D phase shift $\Delta\phi(x, \omega)$ is extracted in the same way as with all other SSSI interferograms [14,15], yielding $\Delta\phi(x, \tau) \propto I_S(x, \tau)f(x, \tau)$, which is plotted in Fig. 3(b). Here, the horizontal fringes imposed by $f(x, \tau)$ show the time-dependent interference between E_S and \mathcal{E}_i . The spatiotemporal pulse envelope is recovered by low pass image filtering of $\Delta\phi(x, \tau)$ to remove $f(x, \tau)$, yielding $I_S(x, \tau)$ in Fig. 3(c).

Extraction of the spatiotemporal phase $\Delta\Phi(x, \tau)$ is performed by Fourier analysis along x [38],

$$\Delta\Phi(x, \tau) = \arg(\mathcal{F}_k^{-1}\{\mathcal{F}_x\{\Delta\phi(x, \tau)\}\Theta(k)\}), \quad (1)$$

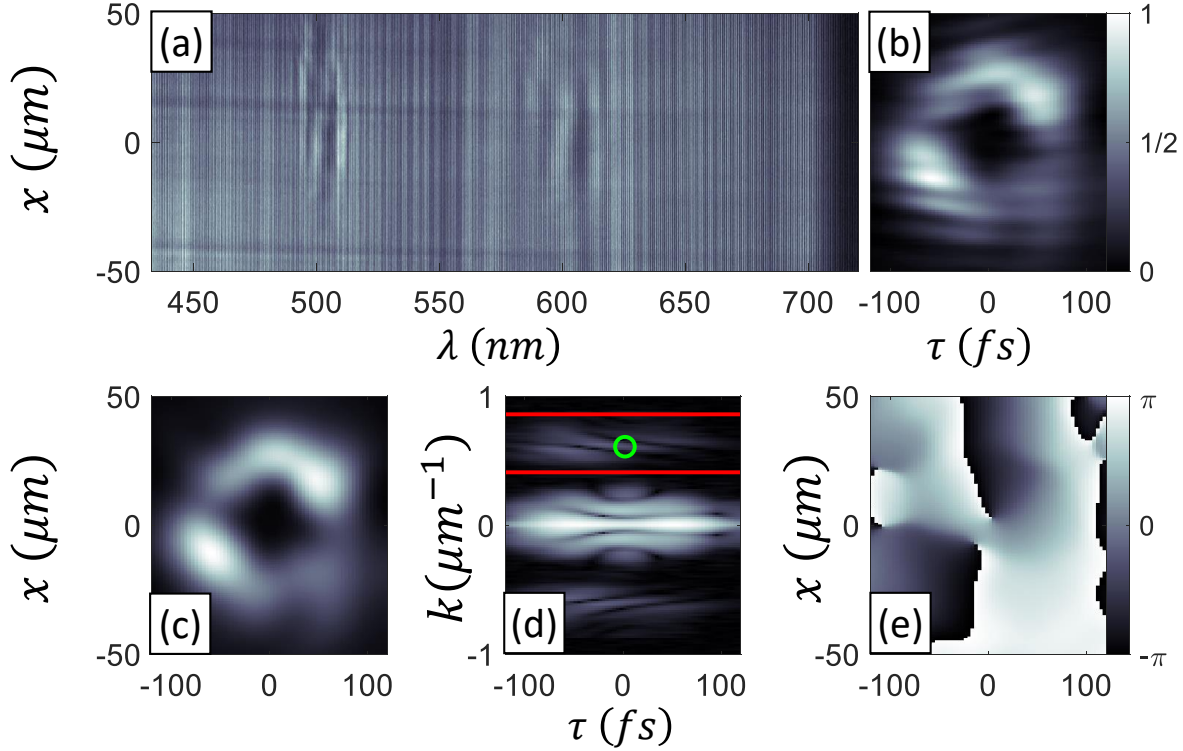


Fig. 3. Measurement of a $l = -2$ STOV-carrying pulse (interferometric reference \mathcal{E}_i at 800nm and 10nm FWHM bandwidth); (a) Raw 1D space-resolved spectral interferogram; (b) extracted $\Delta\phi(x, \tau)$; (c) pulse envelope $I_S(x, \tau)$ from low pass filtering of $\Delta\phi(x, \tau)$; (d) $\log(|\mathcal{F}_x\{\Delta\phi(x, \tau)\}| + 1)$. The red lines show the region to be spectrally windowed and the green circle identifies (k_c, τ_c) for frame averaging; (e) extracted spatiotemporal phase of the pulse, $\Delta\Phi(x, \tau)$.

where $\mathcal{F}_x\{\Delta\phi(x, \tau)\} = \Delta\tilde{\phi}(k, \tau)$ is the Fourier transform along x , $\mathcal{F}_k^{-1}\{\cdot\}$ is the inverse Fourier transform along k , $\Theta(k)$ is a sideband windowing and shifting ($k \rightarrow k - 2\pi/\Lambda$) function, and k is the x -component of the spatial frequency. This is shown in Fig. 3(d) and (e). If the sideband is too close to the k -spectrum of the pulse envelope (which is centered at $k = 0$), $\Theta(k)$ cannot separate the transient grating from the pulse envelope. This necessitates a larger spatial sample and/or finer grating period, considerations that have informed our pump-probe beam geometry.

Even though TG-SSSI is a single-shot method, averaging many shots of a reproducible transient process enables significant enhancement of the signal-to-noise ratio. Before averaging, however, the shot-to-shot shifting of the spatial interference fringes (from mechanical vibrations in the optical setup) must be compensated. The fringes are effectively forced into common alignment by adding a constant phase $\Delta\tilde{\phi}_n(k_c, \tau_c)$ to each frame, giving

$$\Delta\bar{\Phi}(x, \tau) = \arg\left(\frac{1}{N} \sum_{n=1}^N \mathcal{F}_k^{-1}\{[\Delta\tilde{\phi}_n(k, \tau) \times \exp(i\arg(\Delta\tilde{\phi}_n(k_c, \tau_c)))]\Theta(k)\}\right), \quad (2)$$

where $\Delta\tilde{\phi}_n(k, \tau) = \mathcal{F}_x\{\Delta\phi_n(x, \tau)\}$, $\Delta\tilde{\phi}_n(k_c, \tau_c)$ is the constant phase added to frame n to align the fringes, (k_c, τ_c) is a common point across all N frames, and $\Delta\bar{\Phi}(x, \tau)$ is the mean spatiotemporal phase. The point (k_c, τ_c) is chosen at a location in the sideband where the signal is sufficiently larger than the phase noise, otherwise each frame would be offset by a random phase factor.

III. Results and Discussion

To demonstrate TG-SSSI, we used the $4f$ pulse-shaper to generate (a) a Gaussian pulse ($l = 0$, no phase plate), and STOV-carrying pulses with topological charge (b) $l = +1$, (c) $l = -1$, and (d) $l = -2$, using corresponding spiral phase plates in the Fourier plane of the shaper. The columns of Fig. 4 show $\Delta\phi(x, \tau)$, $I_s(x, \tau)$, $f(x, \tau)$, and $\Delta\Phi(x, \tau)$ for pulses carrying $l = 0, \pm 1$, and -2 . For $l = 0$ (row (a)), we see a slight fringe curvature in the transient grating $f(x, \tau)$, indicating a dispersion mismatch between E_s and \mathcal{E}_i . For the $l = \pm 1$ STOVs in rows (b) and (c), $f(x, \tau)$ clearly shows the transient fringe fusing or splitting identifying the opposite phase windings shown in the $\Delta\Phi(x, \tau)$ column. For $l = -2$ (row (d)), one fringe in $f(x, \tau)$ splits into three at the center of the pulse. Upon phase extraction, $\Delta\Phi(x, \tau)$ has two nearby $l = -1$ phase windings rather than a single $l = -2$ winding. We attribute this to a mismatch between the transverse beam dimensions at the Fourier plane of the pulse shaper and the radially independent phase winding of the $l = -2$ phase plate. Since the profile of the beam in the Fourier plane of the shaper (itself dictated by the grating periodicity and cylindrical lens focal length) is slightly elliptical, one of the axes of the phase plate should ideally be scaled to match the ellipticity of the beam. Utilizing a programmable

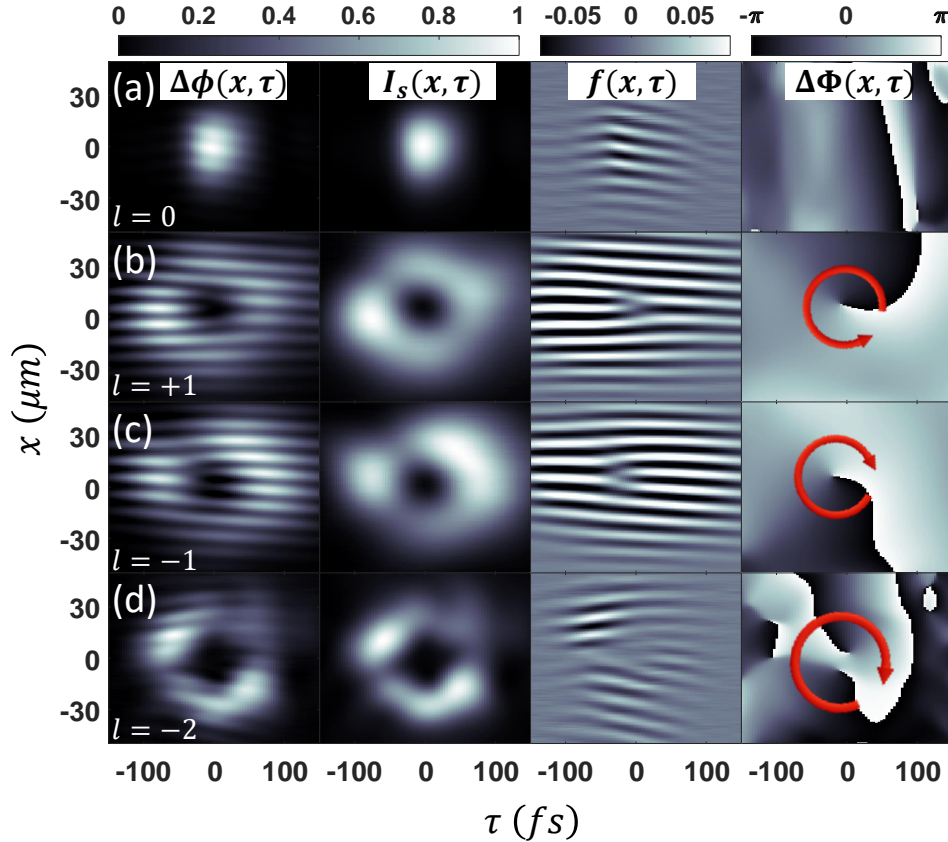


Fig. 4. Experimental results from TG-SSSI after fringe alignment. Columns show the extracted full TG-SSSI signal $\Delta\phi(x, \tau)$, which is low-pass filtered to yield the pulse intensity envelope $I_s(x, \tau)$, or high-pass filtered to give the transient grating $f(x, \tau)$, from which the spatiotemporal phase $\Delta\Phi(x, \tau)$ is extracted. The rows show results for (a) a Gaussian pulse ($l = 0$), (b) a $l = +1$ STOV, (c) a $l = -1$ STOV, and (d) results from an $l = -2$ phase plate. The red arrows denote the direction of increasing spatiotemporal phase.

spatial light modulator rather than a fixed phase plate in the pulse shaper would enable scaling of the phase mask to match the beam profile, making possible the generation of $l = \pm 2$ and even higher order STOVs.

IV. Conclusion

In summary, we have presented a new single-shot diagnostic of ultrashort spatio-temporally structured laser pulses, transient grating single-shot supercontinuum spectral interferometry (TG-SSSI) and have used it to measure simple Gaussian and STOV-carrying pulses generated by a $4f$ pulse-shaper. Among multiple possible applications, TG-SSSI should prove useful in the study of nonlinear propagation, collapse and collapse arrest of intense laser pulses in transparent media, where spatio-temporal optical pulse structures naturally emerge [25]. Finally, we note for experiments where the structured pulse E_S is highly repetitive and reproducible, TG-SSSI could be extended to two spatial dimensions (x and y) by transversely scanning E_{pr}^{out} across the spectrometer entrance slit in the y direction, as is done in 2D+1 SSSI [20], to obtain $I_S(x, y, \tau)$ and $\Delta\Phi(x, y, \tau)$.

Acknowledgements The authors thank I. Larkin for discussions and technical assistance. This work is supported by Air Force Office of Scientific Research (FA9550-16-10121, FA9550-16-10284); Office of Naval Research (N00014-17-1-2705, N00014-20-1-2233); National Science Foundation (PHY2010511).

References

1. F. Salin, P. Georges, G. Roger, and A. Brun, "Single-shot measurement of a 52-fs pulse," *Appl. Opt.* **26**, 4528-4531 (1987).
2. R. Trebino, and D. J. Kane, "Using phase retrieval to measure the intensity and phase of ultrashort pulses: frequency-resolved optical gating," *J. Opt. Soc. Am. A.* **10**, 1101-1111 (1993).
3. D. J. Kane, and R. Trebino, "Single-shot measurement of the intensity and phase of an arbitrary ultrashort pulse by using frequency-resolved optical gating," *Opt. Lett.* **18**, 823-825 (1993).
4. J. N. Sweetser, D. N. Fittinghoff, and R. Trebino, "Transient-grating frequency-resolved optical gating," *Opt. Lett.* **22**, 519-521 (1997).
5. K. W. DeLong, R. Trebino, J. Hunter, and W. E. White, "Frequency-resolved optical gating with the use of second-harmonic generation," *J. Opt. Soc. Am. B.* **11**, 2206-2215 (1994).
6. P. O'Shea, M. Kimmel, X. Gu, and R. Trebino, "Highly simplified device for ultrashort-pulse measurement," *Opt. Lett.* **26**, 932-934 (2001).
7. C. Iaconis and I. A. Walmsley, "Spectral phase interferometry for direct electric-field reconstruction of ultrashort optical pulses," *Opt. Lett.* **23**, 792-794 (1998).
8. P. Baum, S. Lochbrunner, and E. Riedle, "Zero-additional-phase SPIDER: full characterization of visible and sub-20-fs ultraviolet pulses," *Opt. Lett.* **29**, 210-212 (2004).
9. M. Hirasawa, N. Nakagawa, K. Yamamoto, R. Morita, H. Shigekawa, and M. Yamashita, "Sensitivity improvement of spectral phase interferometry for direct electric-field reconstruction for the characterization of low-intensity femtosecond pulses," *Appl. Phys. B.* **74**, s225-s229 (2002).
10. C. Dorrer, P. Londero, and I. A. Walmsley, "Homodyne detection in spectral phase interferometry for direct electric-field reconstruction," *Opt. Lett.* **26**, 1510-1512 (2001).
11. A. Monmayrant, M. Joffre, T. Oksenhendler, R. Herzog, D. Kaplan, and P. Tournois, "Time-domain interferometry for direct electric-field reconstruction by use of an acousto-optic programmable filter and a two-photon detector," *Opt. Lett.* **28**, 278-280 (2003).
12. E. M. Kosik, A. S. Radunsky, I. A. Walmsley, and C. Dorrer, "Interferometric technique for measuring broadband ultrashort pulses at the sampling limit," *Opt. Lett.* **30**, 326-328 (2005).
13. K. Y. Kim, I. Alexeev, and H. M. Milchberg, "Single-shot supercontinuum spectral interferometry," *Appl. Phys. Lett.* **81**, 4124-4126 (2002).

14. J. K. Wahlstrand, S. Zahedpour, and H. M. Milchberg, "Optimizing the time resolution of supercontinuum spectral interferometry," *J. Opt. Soc. Am. B* **33**, 1476-1481 (2016).
15. D. Patel, D. Jang, S. W. Hancock, H. M. Milchberg, and K. Y. Kim, "Simplified single-shot supercontinuum spectral interferometry," *Optics Express* **28**, 11023-11032 (2020).
16. Z. Guang, M. Rhodes, M. Davis, and R. Trebino, "Complete characterization of a spatiotemporally complex pulse by an improved single-frame pulse-measurement technique," *J. Opt. Soc. Am. B* **31**, 2736-2743 (2014).
17. M. Louisy, C. Guo, L. Neoričić, S. Zhong, A. L'Huillier, C. L. Arnold, and M. Miranda, "Compact single-shot d-scan setup for the characterization of few-cycle laser pulses," *Appl. Opt.* **56**, 9084-9089 (2017).
18. S. P. Le Blanc, E. W. Gaul, N. H. Matlis, A. Rundquist, and M. C. Downer, "Single-shot measurement of temporal phase shifts by frequency-domain holography," *Opt. Lett.* **25**, 764-766 (2000).
19. J. P. Geindre, P. Audebert, A. Rousse, F. Fallières, J. C. Gauthier, A. Mysyrowicz, A. Dos Santos, G. Hamoniaux, and A. Antonetti, "Frequency-domain interferometer for measuring the phase and amplitude of a femtosecond pulse probing a laser-produced plasma," *Opt. Lett.* **23**, 1997-1999 (1994).
20. J. K. Wahlstrand, S. Zahedpour, A. Bahl, M. Kolesik, and H. M. Milchberg, "Bound-electron nonlinearity beyond the ionization threshold," *Phys. Rev. Lett.* **120**, 183901 (2018).
21. Y. H. Chen, S. Varma, A. York, and H. M. Milchberg, "Single-shot, space- and time-resolved measurement of rotational wavepacket revivals in H₂, D₂, N₂, O₂, and N₂O," *Opt. Exp.* **15**, 11341-11357 (2007).
22. J. K. Wahlstrand, S. Zahedpour, Y.-H. Cheng, J. P. Palastro, and H. M. Milchberg, "Absolute measurement of the ultrafast nonlinear electronic and rovibrational response in H₂ and D₂," *Phys. Rev. A* **92**, 063828 (2015).
23. S. Zahedpour, S. W. Hancock, and H. M. Milchberg, "Ultrashort infrared 2.5-11 μm pulses: spatiotemporal profiles and absolute nonlinear response of air constituents," *Opt. Lett.* **44**, 843-846 (2019).
24. S. W. Hancock, S. Zahedpour, A. Goffin, and H. M. Milchberg, "Free-space propagation of spatiotemporal optical vortices," *Optica* **6**, 1547-1553 (2019).
25. N. Jhajj, I. Larkin, E. W. Rosenthal, S. Zahedpour, J. K. Wahlstrand, and H. M. Milchberg, "Spatiotemporal Optical Vortices," *Phys. Rev. X* **6**, 031037 (2016).
26. L. Allen, M. W. Beijersbergen, R. J. C. Spreeuw, and J. P. Woerdman, "Orbital angular momentum of light and the transformation of Laguerre-Gaussian laser modes," *Phys. Rev. A* **45**, 8185 (1992).
27. M. A. Porras, "Upper Bound to the Orbital Angular Momentum Carried by an Ultrashort Pulse," *Phys. Rev. Lett.* **122**, 123904 (2019).
28. L. Marrucci, C. Manzo, and D. Paparo, "Optical Spin-to-Orbit Angular Momentum Conversion in Inhomogeneous Anisotropic Media," *Phys. Rev. Lett.* **96**, 163905 (2006).
29. S. Carbajo, E. Granados, D. Schimpf, A. Sell, K.-H. Hong, J. Moses, and F. X. Kärtner, "Efficient generation of ultra-intense few-cycle radially polarized laser pulses," *Opt. Lett.* **39**, 2487-2490 (2014).
30. J. P. Heritage, R. N. Thurston, W. J. Tomlinson, A. M. Weiner, and R. H. Stolen, "Spectral windowing of frequency-modulated optical pulses in a grating compressor," *Appl. Phys. Lett.* **47**, 87-89 (1985).
31. A. M. Weiner, J. P. Heritage, and E. M. Kirschner, "High-resolution femtosecond pulse shaping," *J. Opt. Soc. Am. B* **5**, 1563-1572 (1988).
32. A. M. Weiner, and D. E. Leaird, "Generation of terahertz-rate trains of femtosecond pulses by phase-only filtering," *Opt. Lett.* **15**, 51-53 (1990).
33. N. Jhajj, "Hydrodynamic and electrodynamic implications of optical femtosecond filamentation," Ph.D. dissertation (University of Maryland, 2017), <http://drum.lib.umd.edu/handle/1903/19973>, Chap. 5.
34. S. Zahedpour, S. W. Hancock, and H. M. Milchberg, "Direct measurement of linearly imposed spatiotemporal optical vortices (STOVs)," in *Frontiers in Optics + Laser Science APS/DLS, OSA Technical Digest (Optical Society of America, 2019)*, paper FW5F.5.
35. W. R. Klein and B. D. Cook, "Unified Approach to Ultrasonic Light Diffraction," *IEEE Trans. Sonics Ultrason.* **14**, 123-134 (1967).
36. A. Couairon, E. Brambilla, T. Corti, D. Majus, O. de J. Ramirez-Gongora, and M. Kolesik, "Practitioner's guide to laser pulse propagation models and simulation," *Eur. Phys. J. Special Topics* **199**, 5 (2011).
37. M. Kolesik and J. V. Moloney, "Nonlinear optical pulse propagation simulation: From Maxwell's to unidirectional equations," *Phys. Rev. E* **70**, 036604 (2004).